Proceedings of ALGORITMY 2020
pp. 101–110

CFD SIMULATION AND EXPERIMENTAL ANALYSIS OF FLUIDIZATION IN A MODEL OF AN OXYFUEL FLUIDIZED BED BOILER

M. BENEŠ, P. EICHLER, J. KLINKOVSKÝ, M. KOLÁŘ, T. SMEJKAL, J. SOLOVSKÝ, P. STRACHOTA, A. ŽÁK* AND J. HRDLIČKA, P. SKOPEC†

Abstract. This contribution introduces the methods and tools allowing the validation of a CFD simulator of an oxyfuel bubbling fluidized bed boiler by means of measurements obtained from a laboratory-scale fluidization chamber. For simulations, a custom OpenFOAM solver is developed based on the Multiphase Particle-In-Cell framework for handling the fluid-particle and inter-particle interactions. Some of the solver design details are introduced. Thereafter, the experimental device and its operation are described. The experimental results in the form of video recordings of the fluidized bed subject to changing air flow rates are processed by automatic tools. Using this framework, a direct comparison with the simulation results is possible and the coefficients of the Harris-Crighton model of inter-particle stress are fitted to achieve agreement between simulations and experiment. Based on the results, some improvements of both the CFD model and the experimental methods are proposed.

Key words. CFD simulation, fluidized bed boiler, fluidization experiments, image analysis, MP-PIC, oxyfuel combustion

AMS subject classifications. 65Y05, 65M08, 80A22, 74N05

1. Introduction. In industrial energy production, fluidized bed (FB) combustion [3, 16] is a modern and widely used technology providing fuel selection flexibility, heat transfer efficiency, and convenient means of sulfur oxide removal. In contrast to the more traditional pulverized coal boilers, FB boilers can burn fuels with significant fractions of added biomass [10, 6] or even biomass alone. In combination with the emerging oxyfuel combustion [17, 12] technology and CO_2 capture and storage [9], energy production systems with a negative carbon footprint can be designed.

As part of the project aimed at the research of low-carbon energy production technologies (see Acknowledgment), our team is responsible for the development of a complex mathematical model and CFD software useful in the investigation, optimization, and control of the operation of oxyfuel FB boilers. Within the framework of the project, we take advantage of the close collaboration with our colleagues equipped with laboratory-scale devices so that experiments and simulations work in synergy.

In the combustion chamber of a FB boiler, fuel particles and an additional non-combustible granular material such as limestone take part in multiphase flow, combustion, heat transfer and other processes [16] while being maintained in the fluidized state by a sufficiently strong gas flow. In order to observe and investigate the fluidization characteristics of different materials in the cold state, a model of the lower part of the combustion chamber has been built with walls made of transparent plastic. This paper describes the experiments with fluidization of two different materials and the corresponding CFD numerical simulations in attempt to validate the numerical algorithm.

*Dept. of Mathematics, Faculty of Nuclear Sciences and Physical Engineering, Czech Technical University in Prague, (pavel.strachota@fjfi.cvut.cz),

†Dept. of Energy Engineering, Faculty of Mechanical Engineering, Czech Technical University in Prague.

2. Features of the CFD Simulation Software. The CFD solver for multiphase flow, combustion, and thermodynamics is based on a custom OpenFOAM solver named `kotelFoam`, which is loosely connected to the `coalChemistryFoam` solver. The major building blocks of `kotelFoam` have been introduced in our previous paper [4] and the analysis preceding the choice of OpenFOAM as the primary CFD framework is published in [5].

Currently, the features of `kotelFoam` are the following:

- a finite-volume scheme for compressible viscous turbulent flow of flue gas with a custom chemical composition (aimed at oxyfuel conditions where nitrogen represents a minor component whereas CO_2 is present in high concentrations),
- the Multiphase Particle-in-Cell (MP-PIC) method [2, 13, 14, 11] for simulating the dynamics of Lagrangian parcels of the non-combustible granular bed material with
  - the Gidaspow–Ergun–Wen&Yu drag model [7, 8] for gas-solid momentum transfer,
  - the pressure gradient term that accounts for the forces exerted on the particles by the gas pressure,
  - the modified Harris–Crighton model for inter-particle stress τ [13] in the form

$$\tau = \frac{P_p \alpha_p^{\beta}}{\max\left[(\alpha_{\mathrm{CP}} - \alpha_p)\,,\, \varepsilon(1-\alpha_p)\right]}, \tag{2.1}$$

    where α_p is the solid volume fraction, α_{CP} is the particle volume fraction at close packing and P_p, β, and ε are tunable constants (see Table 3.2).
- Lagrangian simulation of fuel parcels based on `coalCloud` (which is derived from `kinematicCloud`),
- chemistry and heat transfer model based on the features of `coalChemistryFoam`,
- correct representation of the gas volume fraction in all equations for the gas phase,
- ideal gas equation of state.

The instability in parallel computations has been resolved since the publication of [4]. The model is currently able to simulate all regimes of fluidization:

- fixed bed with particles at rest and solid volume fraction at the packing limit,
- bubbling bed with high solid volume fraction in the lower part of the combustion chamber,
- circulating fluidized bed with dilute solid particles across the whole combustion chamber.

3. Methodology. In the following, the experimental device and its function are first described. Next, the design of the experiment and the corresponding simulation is laid out.

The Experimental Fluidization Chamber. The main part of the experimental device is a fluidization chamber in the form of a column with rectangular cross section, as shown in Figure 3.1. At the bottom of the fluidization chamber, there is a perforated plate (the distributor) with an additional fine grille. The given amount of granular material is placed on top of the distributor so that its particles cannot fall through the grille. Another plastic block under the distributor (the windbox) contains an air inlet at the bottom. The air outlet is at the side wall just under the top of the fluidization chamber and it is kept at atmospheric pressure.

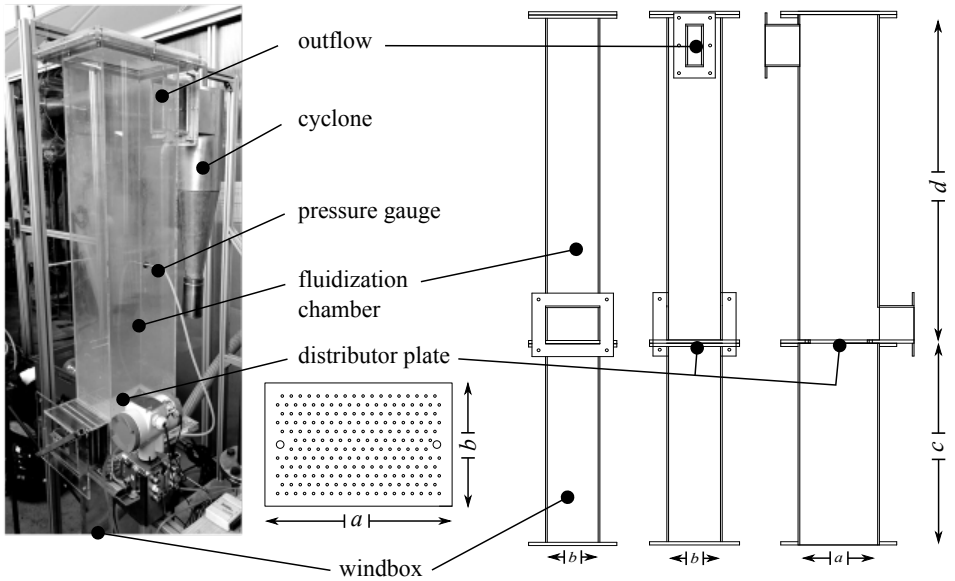

FIG. 3.1. *A photograph and a schematic drawing of the experimental fluidization device with a plastic fluidization chamber. The inner dimensions are* $a = 225$ *mm,* $b = 150$ *mm,* $c = 640$ *mm,* $d = 1000$ *mm. The distributor plate contains 201 holes with the diameter of* 3 *mm. The particles escaping the fluidization chamber are collected in the small container under the cyclone.*

Once the air inflow is turned on, the windbox together with the distributor ensure a (more or less) uniform distribution of the airflow across the whole bottom of the combustion chamber. The air proceeds through the pores between the particles to the freeboard above the layer of the granular material. As the airflow is increased, the gas superficial velocity reaches the minimum fluidization velocity v_{mf} [1] and the airflow begins to lift the solid particles. This is termed the *onset of fluidization*. With further increase in airflow, air bubbles start to develop in the whole layer of granular material and the bubbling fluidized bed is created. The aggregate pressure drop induced by the distributor and the bed of granular material is measured by the pressure gauges. The onset of fluidization can be detected as the moment when this pressure drop stops growing with increasing airflow.

Experiment Setup. The experiments were performed to assess the fluidization behavior and determine the onset of fluidization for two different granular materials: sand and LECA (lightweight expanded clay aggregate). The properties of these materials and the amounts used are summarized in Table 3.1. Once each material was put into the fluidization chamber, the airflow was turned on at the minimum rate. Subsequently, the rate was gradually increased to the maximum value and then decreased again down to zero. In both cases, video footage was taken by a camera mounted at a fixed position in front of the wider wall of the fluidization chamber.

Table 3.1 also contains data related to the course of the experiment. In particular, note that the maximum air flow rate is dependent on the pressure drop above the distributor, i.e. it is slightly different for both experiments. The minimum fluidization velocity has been calculated using several different correlations from the review article

TABLE 3.1
Material properties and experiment setup. The quantities marked with "∗" were also used as simulation parameters in combination with the setup summarized in Table 3.2.

	Units	Sand	LECA
Vendor designation	–	ST 03-3	Liapor LWA 0-2
Mean particle diameter d *	mm	0.8	1.2
Material density ρ_s *	$\mathrm{kg \cdot m^{-3}}$	2650	1050
Bulk density	$\mathrm{kg \cdot m^{-3}}$	∼1550	575
Max. solid volume fraction α_{CP} *	1	∼0.58	0.55
Min. fluidization velocity v_{mf} [1]	$\mathrm{m \cdot s^{-1}}$	0.39 − 0.46	0.34 − 0.38
Amount of solid *	kg	3.29	2.49
Bed height at rest	cm	6.28	12.83
Max. air flow rate	$\mathrm{m^3 \cdot h^{-1}}$	146	149
Max. superficial velocity $v_{g,\mathrm{in}}$ at inlet	$\mathrm{m \cdot s^{-1}}$	1.135	1.144
Temperature *	°C	15	15

[1] and a range of the obtained values is presented.

Simulations Setup. For simulations, the `kotelFoam` solver has been restricted to operate at a constant temperature. No combustible material, no chemical reactions and no heat transfer were present. The computational domain is a block representing the fluidization chamber only, with dimensions a, b, d along the x, z, y coordinate axes, respectively, equal to those shown in Figure 3.1. The whole bottom of the domain is treated as inlet and a uniform value of superficial air velocity $v_{g,\mathrm{in}}$ is prescribed as the boundary condition. This approximates the behavior of the distributor. The local inhomogeneities of the flow (caused by the small holes in the distributor plate) are neglected. For simplicity, the outflow is realized through the whole top side of the domain where the atmospheric pressure is prescribed.

In the initial condition, the given amount of material is dispersed in the form of computational parcels in the lower part of the computational domain. It is not possible to prescribe an initial condition in the form of the layer of particles lying at the bottom next to each other. The distances of the parcels must be large enough so that the MP-PIC inter-particle stress correlation does not exhibit singularities, i.e. the local values of solid volume fraction α_p must be significantly below the packing limit α_{CP} (see Table 3.1). If the simulation is launched without air flow ($v_{g,\mathrm{in}} = 0$), the fixed packed bed ($\alpha_p \to \alpha_{\mathrm{CP}}$) develops once the equilibrium between gravity and inter-particle stress is reached.

Validation Methods. To adjust the model parameters and validate it against the experiments, two main characteristics observable from the experiments were considered:

1. the onset of fluidization and its comparison with the theoretical value of minimum fluidization velocity v_{mf},
2. the height of the bubbling bed and its dependence on the superficial gas velocity at inlet $v_{g,\mathrm{in}}$.

The a priori unknown model parameters subject to adjustment were the values of P_p, β, and ε in the Harris–Crighton model for inter-particle stress. The first aim was to achieve a correct bed height at rest and the values of α_{CP} given in Table 3.1. After that, the parameters were tuned with respect to the onset of fluidization and the bed

TABLE 3.2

Settings of the `kotelFoam` *solver. In addition, the data from Table 3.1 were also used to set up the simulations. The other details (finite volume numerical scheme settings etc.) not given in this table are identical to the default setup of the* `coalChemistryFoam` *solver.*

	Units	Sand	LECA
Mesh DOF	1	$25 \times 15 \times 100$	
Number of parcels	1	100,000	
Particles per parcel	1	43	26
Air turbulence model	–	k-ε RAS	
Harris–Crighton coef. P_p	Pa	100	100
Harris–Crighton coef. β	–	2.0	3.5
Harris–Crighton coef. ε	–	1×10^{-7}	
Pressure p at outflow	Pa	1×10^5	
Gravity acceleration	$\mathrm{m} \cdot \mathrm{s}^{-2}$	9.81	
Minimum velocity $v_{g,\mathrm{in}}$ at inlet	$\mathrm{m} \cdot \mathrm{s}^{-1}$	0.5	0.5
Maximum velocity $v_{g,\mathrm{in}}$ at inlet	$\mathrm{m} \cdot \mathrm{s}^{-1}$	1.3	1.4
Velocity increase step	$\mathrm{m} \cdot \mathrm{s}^{-1}$	0.2	0.1
Final time	s	4	4

height. First, the parameter space $\beta \in \{1, 2, \ldots, 6\}$ and $P_p \in \{10, 50, 100, 500, 1000\}$ was traversed and the best combination was chosen for each material separately. To find the final values of β, a finer sampling with the step 0.5 was used. ε in (2.1) is a regularization parameter only and keeping its default value was sufficient.

Unlike the course of the experiment, a sequence of individual simulations with different values of $v_{g,\mathrm{in}}$ was performed for each material. The summary of computational parameters is given in Table 3.2 and it already contains the best fit of the values of P_p, β .

4. Results. In this section, the results obtained by the simulations using the settings in Tables 3.1 and 3.2 are presented, i.e. only the best choice of P_p, β. The image processing techniques employed to enable the comparison with the experimental data are explained as well.

Experimental Data Processing. The video footage taken during the experiments was converted to a sequence of frames and simple image processing techniques were used to detect the average bed height inside the fluidization chamber. LECA is very dark in contrast to the rest of the image and thus a straightforward thresholding technique could be used to detect the bed level. In the case of sand, the most easily detectable region in the images was the thin layer on the top of the fluidized bed that was the brightest due to light conditions. These observations led to (manually) choosing the suitable brightness thresholds independently for sand and LECA. To find the bed height, thresholding together with the calculation of the center of mass of the segmented region were employed. For the bed at rest, this introduced a small bed height offset which was subsequently used to correct the results. As the light conditions were constant over the course of each experiment, the same algorithm could be applied to all frames of each video.

In addition, the frames were analyzed visually in 1 second intervals to detect the highest point of the fluidized bed. At the same time, the air flow rate measurement by the rotameter was recorded and the superficial gas velocity at inlet $v_{g,\mathrm{in}}$ was calculated.

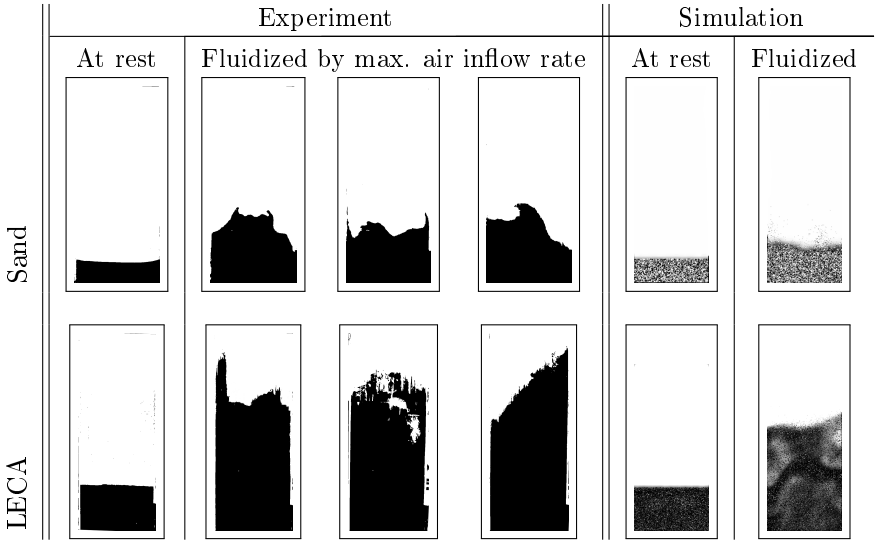

FIG. 4.1. *Qualitative behavior of the fluidized bed of sand and LECA. For experiments with each of the material, one image of the bed at rest and three images during the chaotic bubbling fluidization were taken. The images were processed by thresholding based on the color of the bed material and the environment, with some manual postprocessing to remove artifacts. The simulation results show the visualization of the computational parcels. In the background, the image of the solid volume fraction α_p in a planar section through the center of the fluidization chamber indicates the regions of high particle concentration in dark gray. All images show approximately the same view of the front side of the the lower part of the fluidization chamber.*

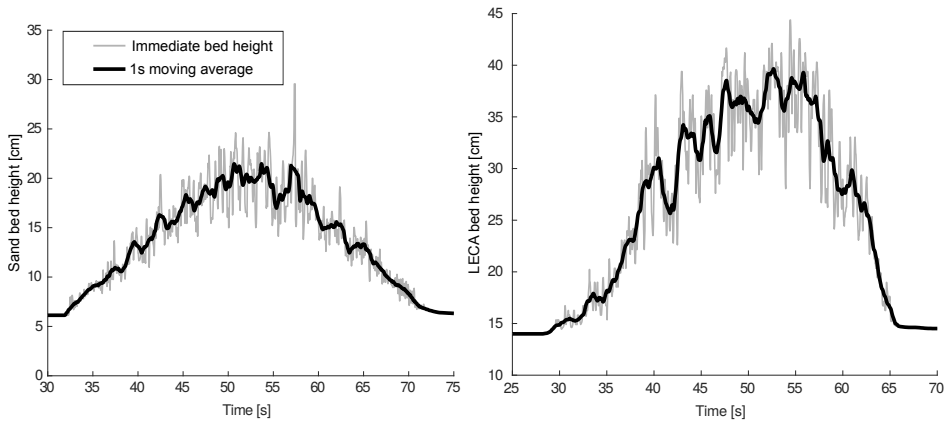

FIG. 4.2. *Results of the automatic analysis of the bed height of sand and LECA during the course of the experiment. Sand bed height measurements have been adjusted to the correct sand bed height at rest.*

Figure 4.1 provides an idea of the dynamics of the fluidized bed and the information available in the videos. The automatically detected time evolution of the average bed height is demonstrated in Figure 4.2. The maximum and average bed height plotted with respect to the superficial air velocity $v_{g,\text{in}}$ is shown in Figure 4.3.

Simulation Results. For each material and for each value of $v_{g,\text{in}}$ in the range given in Table 3.2, a 4 second simulation was performed. In the first approximately

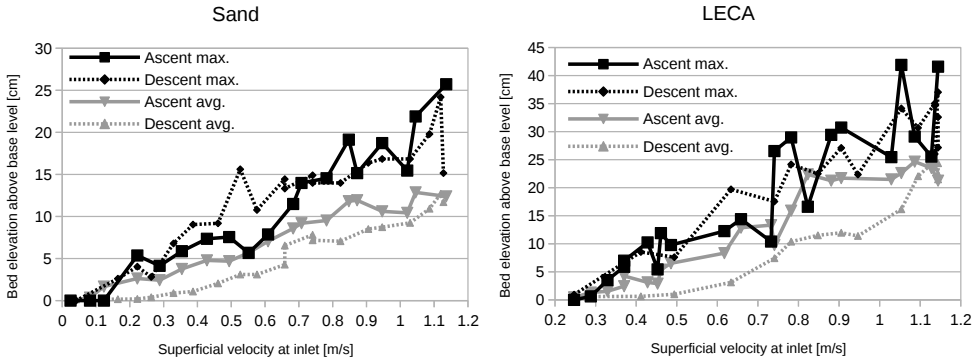

FIG. 4.3. *Bed elevation above base level related to the inlet superficial velocity $v_{g,in}$ during the periods of air flow rate increase (ascent) and decrease (descent). The velocity has been calculated from the air flow rate measured by the rotameter. The maximum values were obtained from the video frames in 1 s intervals by visually detecting the highest point reached by the bed material. The average values were calculated as 1 s averages from the automatically obtained data (see Figure 4.2). For both materials, the average values exhibit a hysteretic behavior.*

1 s, the bed fell down from its dispersed state given by the initial condition. During the last second of the physical time, no effect of the initial condition was observable. Using 20 time snapshots uniformly sampling this time period, the bed height was obtained automatically from the values of α_p (which are interpolated onto the mesh from the particle positions in MP-PIC). The values of α_p were processed in the section through the center of the fluidization chamber and 1D profiles of the bed height were obtained for each of the time snapshots, as demonstrated in Figure 4.4. Afterward, the following overall values were calculated:

- **AVG.** bed height = average both over the 1D profile and over time.
- **max.** bed height = maximum over the 1D profile and average over time. This was used for LECA where the simulations exhibit a very chaotic behavior and smaller bubbles rise alternately at different places of the chamber. It seems to be comparable to the average values automatically obtained from the experiments as the video from the side displays the bed all through the fluidization chamber (it actually makes a "maximum" across the z direction).
- **MAX.** bed height = maximum over both the 1D profile and over time. This was used for sand where the simulations exhibit a pulsating behavior. Large flat bubbles emerge from the bottom and periodically move the bed level up and down.

The obtained results and comparison with the measured data can be seen in Figure 4.5. In contrast to the experiment, the fluidization does not occur for $v_{g,\mathrm{in}} < 0.5\ \mathrm{m} \cdot \mathrm{s}^{-1}$. Beyond that value, the simulation results are comparable to the experimental data.

For all simulations, the HELIOS cluster at the Department of Mathematics, FNSPE CTU Prague was used. Each individual simulation took from 2 to 3 hours of wall time (the higher the value of $v_{g,\mathrm{in}}$, the more computational time is needed), using 64 MPI processes distributed to two compute nodes. Each node is equipped with two 16-core AMD EPYC 7281@2.1GHz CPUs with SMT mode disabled.

5. Discussion and Conclusion. The presented methods and results demonstrate that the MP-PIC based CFD solver is capable of producing both qualitatively and quantitatively comparable results. However, we see room for improvement or more careful investigation in a number of areas.

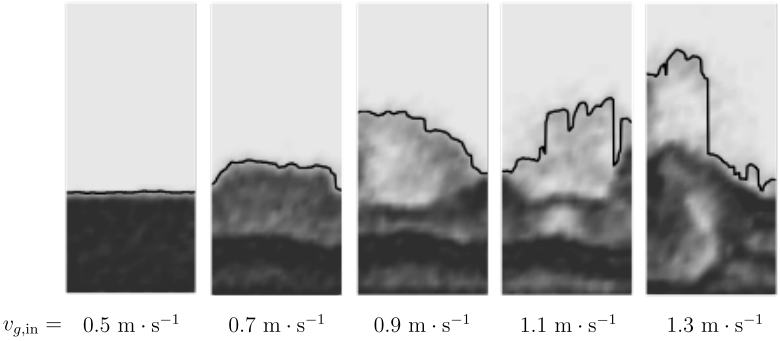

FIG. 4.4. *Sample snapshots demonstrating the function of the bed height detection algorithm. Simulation results for different values of $v_{g,in}$, planar section through the center (plane $z = b/2$) of the lower part of the fluidization chamber.*

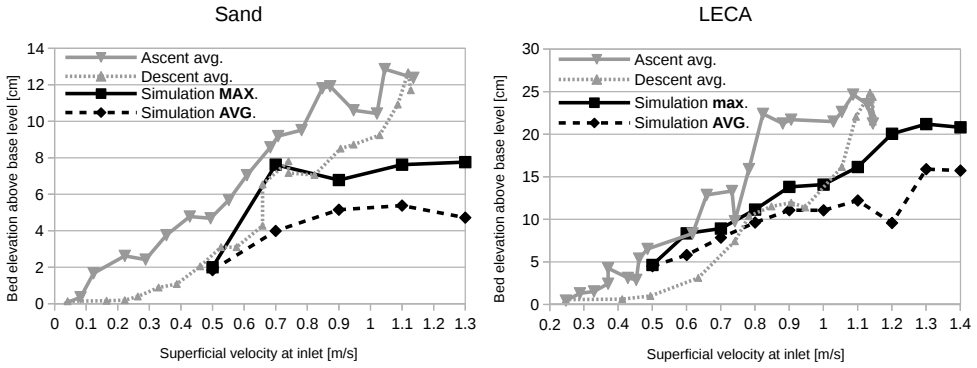

FIG. 4.5. *Bed elevation above base level related to inlet superficial velocity $v_{g,in}$. Comparison of the simulation results with the average bed height detected from experimental data (see Figure 4.3). Note the symbols **AVG**, **max**, **MAX** and their explanation in Section 4.*

In terms of the simulations, the performed tests showed that in most settings of the Harris–Crighton model, the onset of fluidization appeared for much larger values of $v_{g,\mathrm{in}}$ than expected from both the experiment and the calculation of the minimum fluidization velocity (see Table 3.1). This issue partially remains even for the final setup of the Harris–Crighton model.

In the effort to improve the results, it was natural to choose different drag models available in OpenFOAM (e.g. the Syamlal–O'Brien model [15]), which was possible due to the design of the `kotelFoam` solver [5]. Surprisingly, the results obtained with the other drag models were almost identical. On the other hand, it remains to investigate the role of the non-sphericity of the particles which has not been taken into account yet.

Neglecting the details of the flow through the distributor plate may be another source of the discrepancy between the experiments and the simulations. In reality, high speed jets of air appear above the holes which may theoretically change the fluidization behavior. However, preliminary simulations with the detailed geometry of the distributor were made (in a model that only includes a small part of the fluidization chamber) and their results do not indicate any significant effect in this

direction.

In terms of the experiments, the main shortcoming stems from the fact that air flow rate change was too rapid. As a consequence, for example, the onset of fluidization cannot be determined reliably. For the desired use, we would appreciate a series of experiments with different air flow rates that would be sustained for a longer time. In addition, covering the back side of the fluidization chamber by a uniformly colored material and improving the lighting conditions would contribute to the better quality of the video recording, which would be more suitable for automatic processing. Preparation of experiments using a high-frequency camera for recording is already under way.

In conclusion, this work introduces a framework of a combined experimental and computational investigation of fluidization phenomena in fluidized bed boilers. It elaborates the methods of validating the results of both approaches and sets out ideas for their further improvement.

Acknowledgments. This work was supported by the Ministry of Education, Youth and Sports of the Czech Republic under the OP RDE grant number CZ.02.1.01/0.0 /0.0/16_019/0000753 "Research centre for low-carbon energy technologies".

REFERENCES

[1] A. Anantharaman, R. A. Cocco, and J. W. Chew. Evaluation of correlations for minimum fluidization velocity (U_{mf}) in gas-solid fluidization. *Powder Technol.*, 323:454–485, 2018.

[2] M. J. Andrews and P. J. O'Rourke. The multiphase particle-in-cell (MP-PIC) method for dense particulate flows. *Int. J. Multiphase Flow*, 22(2):379–402, 1996.

[3] P. Basu. *Combustion and Gasification in Fluidized Beds.* CRC Press, 2006.

[4] M. Beneš, P. Eichler, J. Klinkovský, M. Kolář, J. Solovský, P. Strachota, and A. Žák. Modeling and simulation of bed dynamics in oxyfuel fluidized bed boilers. In *Numerical Mathematics and Advanced Applications ENUMATH 2019*, 2020. to appear.

[5] M. Beneš, P. Eichler, J. Klinkovský, M. Kolář, J. Solovský, P. Strachota, and A. Žák. Numerical simulation of fluidization for applications in oxyfuel combustion. *Discrete. Cont. Dyn. S. S*, online-first:1–15, 2020.

[6] M. Beneš, P. Strachota, R. Máca, V. Havlena, and J. Mach. A quasi-1D model of biomass co-firing in a circulating fluidized bed boiler. In J. Fuhrmann, M. Ohlberger, and C. Rohde, editors, *Finite Volumes for Complex Applications VII - Elliptic, Parabolic, and Hyperbolic Problems*, volume 78 of *Springer Proceedings in Mathematics & Statistics*, pages 791–799. Springer, 2014.

[7] D. Gidaspow. *Multiphase Flow and Fluidization: Continuum and Kinetic Theory Description.* Academic Press, 1994.

[8] Y. Liu and O. Hinrichsen. CFD modeling of bubbling fluidized beds using OpenFOAM® : Model validation and comparison of TVD differencing schemes. *Computers and Chemical Engineering*, 69:75–88, 2014.

[9] M. M. Maroto-Valer, editor. *Developments and innovation in carbon dioxide (CO_2) capture and storage technology.* Woodhead Publishing, 2010.

[10] S. Mehmood, B. V. Reddy, and M. A. Rosen. Energy analysis of a biomass co-firing based pulverized coal power generation system. *Sustainability*, 4:462–490, 2012.

[11] P. J. O'Rourke, P. P. Zhao, and D. M. Snider. A model for collisional exchange in gas/liquid/solid fluidized beds. *Chem. Eng. Sci.*, 64(8):1784–1797, 2009.

[12] F. Sher, M. A. Pans, C. Sun, C. Snape, and H. Liu. Oxy-fuel combustion study of biomass fuels in a 20 kw fluidized bed combustor. *Fuel*, 215:778–786, 2018.

[13] D. M. Snider. An incompressible three-dimensional multiphase particle-in-cell model for dense particle flows. *J. Comput. Phys.*, 170(2):523–549, 2001.

[14] D. M. Snider and P. J. O'Rourke. The multiphase particle-in-cell (MP-PIC) method for dense particle flow. In *Computational Gas-Solids Flows and Reacting Systems: Theory, Methods and Practice*, pages 277–314. IGI Global, 2011.

[15] M. Syamlal. The particle-particle drag term in a multiparticle model of fluidization. Topical Report DOE/MC/21353-2373, NTIS/DE87006500, National Technical Information Service, Springfield, VA, 1987.

[16] W.-C. Yang, editor. *Handbook of Fluidization and Fluid-Particle Systems.* Marcel Dekker, 2003.

[17] L. Zheng, editor. *Oxy-fuel combustion for power generation and carbon dioxide (CO_2) capture.* Woodhead Publishing, 2011.